Membranes for spontaneous separation of pedestrian counterflows

S. KOYAMA, D. INOUE, A. OKADA and H. YOSHIDA (iD)

Toyota Central R&D Labs., Inc. - Bunkyo-ku, Tokyo 112-0004, Japan

Abstract – Designing efficient traffic lanes for pedestrians is a critical aspect of urban planning as walking remains the most common form of mobility among the increasingly diverse methods of transportation. Herein, we investigate pedestrian counterflows in a straight corridor, in which two groups of people are walking in opposite directions. We demonstrate, using a molecular dynamics approach applying the social force model, that a simple array of obstacles improves flow rates by producing flow separations even in crowded situations. We also report on a developed model describing the separation behavior that regards an array of obstacles as a membrane and induces spontaneous separation of pedestrians groups. When appropriately designed, those obstacles are fully capable of controlling the filtering direction so that pedestrians tend to keep moving to their left (or right) spontaneously. These results have the potential to provide useful guidelines for industrial designs aimed at improving ubiquitous human mobility.

Introduction. – Modern transportation systems are becoming increasingly complex and often require different time and spatial scales, as represented by the rapid growth of the diverse transportation methods and mobility technologies [1,2]. Since there are still numerous phenomena that are not fully understood within each of such transportation systems, both experimental and theoretical studies aimed at understanding such phenomena have been performed continuously [3,4]. Among the different transportation methods, walking remains the most fundamental, so pedestrian flows have been widely studied [5–8]. In typical experimental studies, pedestrian trajectories are observed and analyzed by recording their motions with video cameras or using laser measurements [9–16]. On the other hand, theoretical approaches have also been used to gain a systematic understanding of observed pedestrian behaviors and/or for predicting the pedestrian flows under various circumstances [17–21]. For example, the so-called social force model, first proposed by Helbing and Molnár [22], is one of the most widely used theoretical approaches to model pedestrian movements, which enables us to simulate flows using molecular dynamics [23–27].

In the present study, we also employ the social force model to investigate pedestrian behaviors in a straight corridor in which two groups of people are walking in opposite directions. Similar situations with two groups of particles moving in opposite directions have been extensively studied in the context of lane and pattern formations not only of pedestrians [28,29] but also of various physical particles, such as charged colloids [30–32], microswimmers [33], and plasmas [34,35]. These studies are focused mainly on a bulk system without obstacles. Here we demonstrate that separation-membrane–like obstacles placed along the centerline of a corridor improve flow efficiency even in crowded situations. This is because the presence of those obstacles triggers a spontaneous separation of the pedestrians groups, thereby resulting in an unconscious "keep-left" pedestrian mentality, as illustrated in fig. 1. Although relevant studies have been reported, such as effects of placing columns asymmetrically near an exit [23,36], and a partition line effect controlling the critical density in the jamming transition [37], the enhancement of a pedestrian counterflow by means of particular choices of obstacles is, to our knowledge, new. We also report on the development of a model describing the separation behavior, which is inspired by a reminiscent membrane separating multi-component fluids. These findings related to pedestrian group filtering could potentially provide useful guidelines for improving daily pedestrian flows.
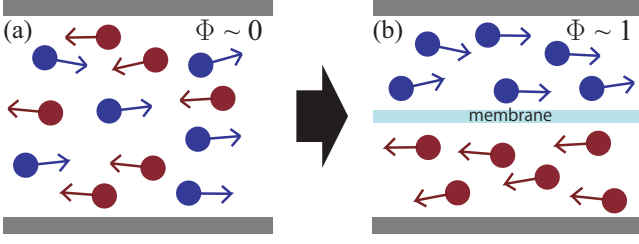
Fig. 1: Pedestrian counterflow separation: (a) flow without filtering membrane and (b) flow separated into two streams using a permeable membrane, which is realized by an array of obstacles. The parameter Φ shown in each figure is an order parameter indicating the degree of lane formation (or separation). See eq. (3) for the precise definition.

Problem. – Here we consider a throng of N pedestrians walking in a straight corridor of width W and length L, as shown in fig. 2(a). In this context, $i \in \mathcal{N}_{+x}$ out of N pedestrians are walking in the $+x$-direction, and the remaining $i \in \mathcal{N}_{-x}$ pedestrians are traveling in the $-x$-direction. Here, we assume $n(\mathcal{N}_{+x}) = n(\mathcal{N}_{-x}) = N/2$. We also assume that the periodic boundary condition in the x-direction, which is set so that the global average density of $\rho_{av} = N/(LW)$, is constant. Such situations, in which a self-organizing lane formation or a clogging phenomenon occurs at high-density points (which is often called jamming transition), have been extensively studied [16,29,38–40].

According to the experiments examining the impacts of congestion in a corridor, pedestrian flow velocities tend to decrease as density increases (see, *e.g.*, ref. [16] and fig. S1 in the Supplemental Information `Supplementarymaterial.pdf` (SI))[1]. In the present study, we consider situations in which an obstacle array is placed along the median line of a corridor to suppress velocity reductions and to control pedestrian flow patterns. To be more specific, we consider elliptic obstacles with major and minor axes of lengths $2a$ and $2b$, respectively, which are placed on the median line of the corridor ($y = 0$) at intervals of L_p. The obstacles are commonly angled, such that the angle between the x-axis and the major axis is φ.

Molecular dynamics simulation. – Before showing simulation results, we will first summarize the model equations used in the molecular dynamics. Each pedestrian is modeled by a spherical particle, the dynamics of which is governed by the following equation of motion:

$$m_i \frac{\mathrm{d}\boldsymbol{v}_i}{\mathrm{d}t} = -m_i \frac{\boldsymbol{v}_i - v_d \boldsymbol{e}_i}{\tau} + \sum_{j \neq i} \boldsymbol{f}_{ij} + \sum_{k \in \text{wall}} \boldsymbol{f}_{ik}^w + \boldsymbol{\xi}_i, \quad (1)$$

where m_i, r_i, and $\boldsymbol{v}_i$ are the mass, radius, and velocity of the i-th particle, respectively. The first term on
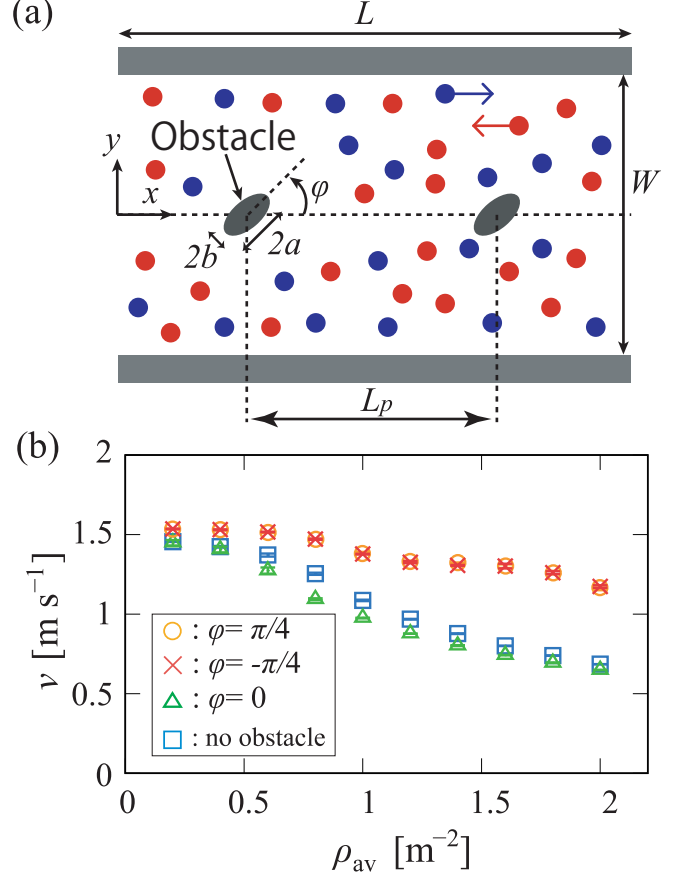
Fig. 2: The present system and fundamental diagram. (a) Schematic of the geometry. (b) Average velocity v *vs.* average density ρ_{av} obtained with the simulations for different situations. The cases with obstacles of $\varphi = 0$ and $\pm\pi/4$ are shown along with the no-obstacle case. The symbols with an error bar indicate the mean value with the standard deviations of no fewer than five samples with different initial conditions. For each run, the value of v is the average over 1.5×10^7 steps with time step $\mathrm{d}t = 0.001$ s, *i.e.*, 1.5×10^4 s.

the right-hand side represents the force driving the pedestrian in the desired direction $\boldsymbol{e}_i$ with velocity v_d and relaxation time τ. The second term is the sum of the pairwise interaction force $\boldsymbol{f}_{ij}$ between pedestrian particles i and j. In the third term, the walls and obstacles are expressed in terms of groups of fixed particles, indexed by $k \in \text{wall}$, with $\boldsymbol{f}_{ik}^w$ being the interaction force between particle i and those fixed particles (see fig. S2 in the SI). Finally, $\boldsymbol{\xi}_i$ indicates the Gaussian white noise satisfying $\langle \boldsymbol{\xi}_i \rangle = \boldsymbol{0}$, $\langle \xi_i(t)\xi_i(t') \rangle = \Xi \boldsymbol{I} \delta(t - t')$, where δ is the Kronecker delta, $\boldsymbol{I}$ is the identity matrix, and Ξ is the noise intensity parameter.

The explicit form of $\boldsymbol{f}_{ij}$ is given by

$$\boldsymbol{f}_{ij} = [A e^{-r'_{ij}/B} - \kappa r'_{ij} u(-r'_{ij})]\boldsymbol{n}_{ij}$$
$$- g r'_{ij} u(-r'_{ij}) \Delta v_{ij}^t \boldsymbol{t}_{ij}, \quad (2)$$

where A, B, κ, and g are the model parameters, and $r'_{ij} = r_{ij} - (r_i + r_j)$, with r_{ij} being the distance between

particle i and j, and $u(z)$ is the Heaviside function, the value of which is unity for $z > 0$ and zero otherwise. The normal unit vector $\boldsymbol{n}_{ij}$ is pointing from the position of particle j to that of i, and the unit vector $\boldsymbol{t}_{ij}$ is in the tangential direction perpendicular to $\boldsymbol{n}_{ij}$. Δv_{ij}^t is the projection of the relative velocity between i and j on $\boldsymbol{t}_{ij}$. The interaction force $\boldsymbol{f}_{ik}^w$ has the same form as eq. (2) with the parameters A and B simply replaced by A_w and B_w.

All the simulations are implemented using the open source code LAMMPS [41]. The source codes in the original package are modified to incorporate the pairwise interactions corresponding to eq. (2) (see sect. S1 of the SI for details). The specific values of parameters used in our simulations are summarized as shown below. The mass of each pedestrian is $m_i = 80\,\mathrm{kg}$ and the diameter of a pedestrian $d_p = 2r_i$ is $0.3\,\mathrm{m}$. We choose $d_w = 1/2\sqrt{2}\,\mathrm{m}$ as the diameter of fixed particles. The model parameters for the pairwise interaction force given in eq. (2) are fixed at $A = A_w = 2000\,\mathrm{N}$, $B = B_w = 0.08\,\mathrm{m}$, $\kappa = 1.2 \times 10^5\,\mathrm{N/m}$, $g = 2.4 \times 10^5\,\mathrm{Pa \cdot s}$, and $\tau = 0.5\,\mathrm{s}$, following ref. [23]. The repulsive force is taken into account only for $r_{ij} < 3.0\,\mathrm{m}$, and is otherwise cut off. The value of pedestrians' desired velocity or terminal velocity is set as $v_d = 1.55\,\mathrm{m/s}$, which is based on the experimental result in ref. [16], and the noise intensity is chosen as $\Xi = 6.63 \times 10^5\,\mathrm{N}^2$ to reproduce the experimental density-velocity relationship discussed below (see fig. S3 in the SI). The initial configuration is constructed with randomly distributed pedestrians, and each simulation runs over 2×10^7 steps with time step $dt = 0.001\,\mathrm{s}$. Note that the simulations set with these parameters reproduce the experimental results well, as shown in fig. S1 in the SI. In the following simulation results, the geometrical parameters are fixed at $L = 20\,\mathrm{m}$, $W = 8\,\mathrm{m}$, $a = 0.7\,\mathrm{m}$, $b = 0.4\,\mathrm{m}$, and $L_p = 10\,\mathrm{m}$ unless otherwise stated.

We show in fig. 2(b) the *fundamental diagram*, namely the density-velocity relation for our system. More precisely, we plot the velocity averaged over the pedestrians walking in the $+x$-direction *vs.* the average density ρ_{av} ($= N/LW$). Here, and in what follows, the time average is taken over 1.5×10^7 steps for each run, and no fewer than five runs with different initial configurations are used to obtain each averaged quantity. In general, pedestrian counterflows under ordinary situations in the absence of obstacles exhibit congestion as density increases, resulting in monotonically decreasing velocity (see, *e.g.*, ref. [16]). This feature is properly captured by our simulation for the no-obstacle case results, which are shown as a reference in fig. 2(b). In the same figure, the case in the presence of obstacles with $\varphi = 0$, *i.e.*, the symmetric obstacles, which have no impact on this fundamental diagram, is also shown. On the other hand, the corridor with emplaced asymmetric obstacles ($\varphi = -\pi/4$ and $\pi/4$) maintains a much higher velocity than that in the previous two cases. The simulation snapshots (see fig. S4 in the SI) imply that this significant velocity enhancement (thus, flux) is a result of lane formations that reduce friction between

particles passing in opposite directions. We also note here that the formed lanes are stable. In other words, once a lane is formed, it tends to occupy the same side of the corridor for a long time. In our simulations, the lanes with emplaced asymmetric obstacles do not change sides during the simulation runs (see fig. S5 in the SI). At this point, we see that the flow structure, *i.e.*, whether or not lanes are formed, plays an essential role in improving traffic flow efficiency.

Next, we investigate the structure of the pedestrian counterflows in the presence of the obstacles in greater detail. In order to quantify the flow structure discussed above, we introduce the order parameter Φ, which is defined as

$$\Phi = \frac{1}{N} \sum_{i=1}^{N} \frac{v_{xi} \cdot y_i}{|v_{xi} \cdot y_i|}, \tag{3}$$

where v_{xi} and y_i are the x component of the velocity and the y component of the position of particle i, respectively [25]. Since $y = 0$ is the median line of the corridor, the value of $v_{xi} \cdot y_i$ is positive when particle i moves in the $+x$-direction in the region $y > 0$. Therefore, $\Phi > 0$ when most pedestrians keep to their left, and similarly $\Phi < 0$ if they keep to their right. The value of Φ vanishes when the pedestrians walking in the opposite directions are uniformly distributed or when the keep-left and keep-right patterns appear with equal probability. This order parameter is normalized such that $|\Phi| = 1$ when the pedestrian flow is perfectly separated into two streams (see fig. 1).

In fig. 3(a), we show the order parameter Φ as a function of the average density ρ_{av} for the situations considered in fig. 2(b), supplemented by the cases of $\varphi = \pi/6$ and $\pi/12$. In the absence of obstacles, the system is purely symmetric about $y = 0$. Hence, we see $\Phi \sim 0$ in the entire range of ρ_{av}. Again, the symmetric obstacles with $\varphi = 0$ do not influence the flow structure. On the other hand, when the obstacles are angled by $\varphi = \pm\pi/4$, $|\Phi| \sim 1$ for the wide range up to $\rho_{\mathrm{av}} \sim 1\,\mathrm{m}^{-2}$, and $|\Phi|$ is larger than 0.75 even for the high densities. In the case of shallower $|\varphi| < \pi/4$ angles, the absolute value of Φ is smaller, but remains significant. In other words, the pedestrian flow exhibits clear self-organization by separating into two groups that keep to their left or to their right as they travel in opposite directions.

In view of the fact that the separation does not occur in the absence of obstacles, the lane formation obtained here is in contrast to that observed in a bulk situation, *i.e.*, in a system without obstacles, for certain parameter ranges (see, *e.g.*, [28,42–44]). In the present case, the asymmetry of obstacles is the main contribution to the lane formation and stabilization. This is confirmed by the symmetric obstacle results, which still do not lead to the stable lane formation. The local interaction with a tilted obstacle transfers a part of momentum in the x-direction into a momentum in the y-direction. Depending on the direction (along x) from which a particle collides, the gained momentum in the y-direction in fact differs.
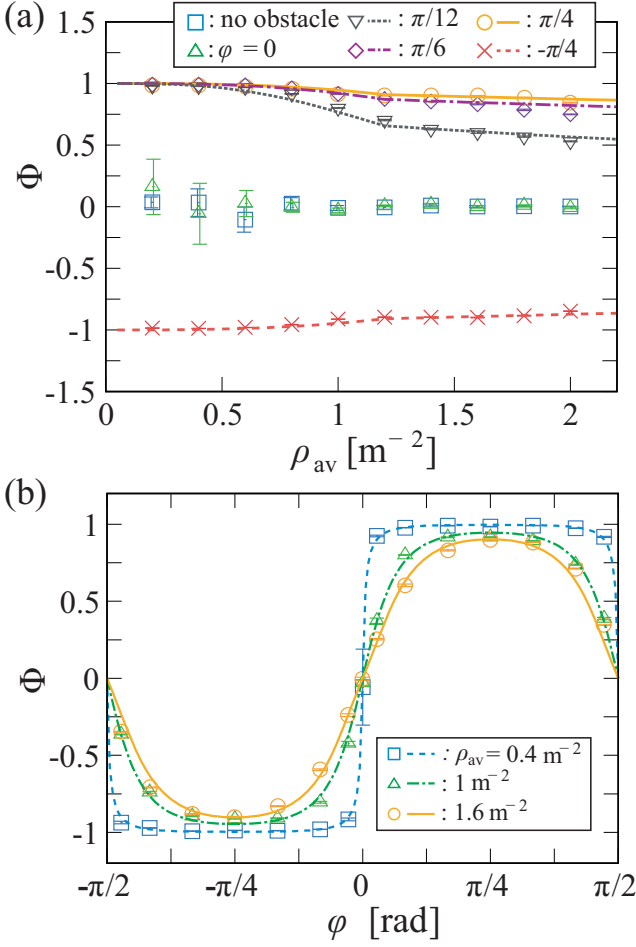
Fig. 3: Order parameter Φ (a) as a function of average density ρ_{av} for various obstacles, and (b) as a function of angle φ of obstacles for various values of ρ_{av}. The symbols indicate the simulation results (see the caption of fig. 2). The predictions of the model given by eq. (4) are shown with lines.

This local imbalance diffuses to the entire region of the corridor, which results in the complete separation with $\Phi \sim 1$ observed in fig. 3(a).

In order to examine the effect of the geometrical parameter in greater detail, we show the relationship between Φ and φ at several values of ρ_{av} in fig. 3(b). The order parameter sign is determined by the angle φ, such that $\Phi > 0$ for $\varphi > 0$ and $\Phi < 0$ for $\varphi < 0$, which confirms that tuning the geometrical parameter enables us not only to induce self-organized lane formations but also to control the flow patterns precisely, *i.e.*, keep them left or keep them right. Figure 3(b) also shows that the control sensitivity to φ depends on the density. More specifically, $|\Phi|$ is rather sensitive for the high density value of $\rho_{\mathrm{av}} = 1.6\,\mathrm{m}^{-2}$, whereas it is robust for the lower density value of $\rho_{\mathrm{av}} = 0.4\,\mathrm{m}^{-2}$.

Membrane model for separation. – We next present a model reproducing the separation behavior of the pedestrian counterflows discussed above. We begin with noting that the role played by the obstacles is

reminiscent of the effects of filtering membranes used to separate different fluid components. Therefore, inspired by the modeling of such filtering membranes [45,46], we now construct a differential equation describing the dynamics of pedestrian concentrations. For simplicity, we assume that the pedestrian density and velocity values are uniform on each side of the membrane. The density of pedestrians walking in the $+x$- or $-x$-direction in the region $y > 0$ is written as $\rho_{y>0}^{\pm x}$. Then, the density in the region $y < 0$ is $\rho_{y<0}^{\pm x} = \rho_{\mathrm{av}}/2 - \rho_{y>0}^{\pm x}$ because the density of people going in each direction in the whole area of $-W/2 < y < W/2$ is $\rho^{+x} = \rho^{-x} = \rho_{\mathrm{av}}/2$. Furthermore, assuming the density of all pedestrians is uniformly distributed, we have $\rho_{y>0}^{+x} + \rho_{y>0}^{-x} = \rho_{\mathrm{av}}/2$. Hence, the system density distribution is fully determined once a governing equation for $\rho_{y>0}^{+x}$ is solved. In the following, $\rho_{y>0}^{+x}$ is simply written as ρ, and the order parameter is expressed as $\Phi = 2(\rho/\rho_{\mathrm{av}} - 1/2)$.

Using the same idea as the model describing concentration variations between two reservoirs separated by a membrane [45,47], we model the behavior of ρ as follows:

$$\frac{\mathrm{d}\rho}{\mathrm{d}t} = \frac{M_1 L}{eS}\left(\frac{\rho_{\mathrm{av}}}{2} - \rho\right) + \frac{M_2 L}{eS}(\rho_{\mathrm{av}} - \rho), \qquad (4)$$

where e is the thickness of the membrane, $S = LW/2$ is the area of interest (now the region $y > 0$). In contrast to the models describing ordinary membranes [45,47], the equation above contains two terms driving the density change characterized by M_1 and M_2; the parameter M_1 controls the driving force that mixes the pedestrians such that the values of ρ in $y > 0$ and $y < 0$ approach. On the other hand, M_2 is the parameter for the driving force that separates the pedestrians moving in the $+x$- and $-x$-directions such that ρ approaches ρ_{av}. The solution of eq. (4) is readily obtained as $\rho = \rho_0 + \rho_1 \exp(-M_1 Lt/eS) + \rho_2 \exp(-M_2 Lt/eS)$, where ρ_1 and ρ_2 are the constants determined from the initial conditions and $\rho_0 = \rho_{\mathrm{av}}(M_1 + 2M_2)/(2M_1 + 2M_2)$ is the stationary solution.

Diffusion phenomena should dominate the physical mechanisms of mixing. Since the analysis of counterflows in the bulk region shows generally increasing diffusion coefficient with increasing density, we assume a functional form for M_1 which increases with density. The diffusion coefficient in the y-direction obtained under wall-free bulk conditions, in comparison with our model for M_1, is found in fig. S6 of the SI, where the linear time dependence of the mean square displacement shows the ordinary diffusion process in the y-direction. On the other hand, in modeling the separating force M_2, we take into account the fact that a certain separation effect is observed even in the low-density region. Hence we assume a constant value for M_2 with respect to ρ_{av}. However, since the separation ability should depend on the the geometrical details of the obstacles forming the membrane, we assume that M_2 depends on the angle φ. We note that a common function of φ is assigned to M_2 for all the results shown below (see fig. S7

in the SI) of which the functional form reflects the shape of obstacles constituting the membrane. The values of Φ obtained from the steady solution of eq. (4) are shown in figs. 3(a) and (b). The results of molecular dynamics simulations, including the variation of decreasing $|\Phi|$ in fig. 3(a), are well captured. In addition, the molecular dynamics results examining the effect of the interval between obstacles L_p are well predicted by the present model with the same parameter set (see fig. S8 in the SI).

From the above comparison, we conclude that the minimum model given in eq. (4), based on the membrane dynamics (with the driving forces chosen appropriately), is capable of predicting the spontaneous separation effect of the pedestrian flow. In addition to the steady-state behavior focused on in the above discussion, the present model was also examined for transient response, and its consistency with the molecular dynamics simulations was confirmed to be within the parameter range where the approximation of eq. (4) was valid, in other words, situations where the corridor area was not too wide and the density to each side of the membrane varies uniformly. More specifically, for the molecular dynamics simulation, we measure the relaxation time taken to reach the steady state exhibiting $|\Phi| \sim 1$, starting from the initial condition with $\Phi = 0$, in which the pedestrians traveling in both directions distribute uniformly in the whole corridor. These results are then compared with the corresponding relaxation time predicted by the model given in eq. (4). The resulting model predictions agree well with the molecular dynamics results under conditions in which W is not too large (see fig. S9 in the SI).

Conclusion. – To summarize, we have shown that simple asymmetric obstacles emplaced in a corridor enable us to control pedestrian flow patterns by inducing self-organizing lane formations. As demonstrated in fig. 2, the structured pedestrian flows are more efficient than those of ordinary unstructured crowds. Thus, the present results could contribute to developing new concepts for engineering corridor designs in ways that create efficient traffic lanes. Here, the asymmetry is generated by designing the geometrical shape of obstacles. However, this is merely an example for realizing the spontaneous separation of pedestrians. The original concept of the "social force" employed in our molecular dynamics simulations includes psychological interactions forces acting effectively on the pedestrians. Therefore, designing *psychological obstacles*, constructed by means of visual effects such as photo-regulation, electronic signage, or some other methods, could provide alternative approaches, and will be included among our future research topics.

Our membrane model for separation has shown good agreements with the molecular dynamics simulation results, as shown in fig. 3. This is an example of the analogies found in multidisciplinary studies, in which a theory established for microscopic physics is used to explain macroscopic phenomena at a length scale that is orders of magnitude higher than the original micro-scale. We believe that our finding suggests a way forward for the field of mobility and transportation, particularly when viewed in tandem with ideas on various unobvious phenomena present in microscopic transportation systems.

$$* \; * \; *$$

REFERENCES

[1] BARBOSA H., BARTHELEMY M., GHOSHAL G., JAMES C. R., LENORMAND M., LOUAIL T., MENEZES R., RAMASCO J. J., SIMINI F. and TOMASINI M., *Phys. Rep.*, **734** (2018) 1.

[2] BARTHELEMY M., *Nat. Rev. Phys.*, **1** (2019) 406.

[3] LV Y., DUAN Y., KANG W., LI Z. and WANG F.-Y., *IEEE Trans. Intell. Transp.*, **16** (2014) 865.

[4] VARGA L., KOVÁCS A., TÓTH G., PAPP I. and NÉDA Z., *PLoS ONE*, **11** (2016) e0148913.

[5] SCOTT A. J., *Socio-Econ. Plan. Sci.*, **8** (1974) 317.

[6] POLUS A., SCHOFER J. L. and USHPIZ A., *J. Transp. Eng.*, **109** (1983) 46.

[7] GIPPS P. G. and MARKSJÖ B., *Math. Comput. Simul.*, **27** (1985) 95.

[8] VIRKLER M. R. and ELAYADATH S., *Transp. Res. Rec.*, **1438** (1994) 51.

[9] SEYFRIED A., STEFFEN B., KLINGSCH W. and BOLTES M., *J. Stat. Mech.*, **2005** (2005) P10002.

[10] HELBING D., JOHANSSON A. and AL-ABIDEEN H. Z., *Phys. Rev. E*, **75** (2007) 046109.

[11] JOHANSSON A., HELBING D., AL-ABIDEEN H. Z. and AL-BOSTA S., *Adv. Complex Syst.*, **11** (2008) 497.

[12] CHATTARAJ U., SEYFRIED A. and CHAKROBORTY P., *Adv. Complex Syst.*, **12** (2009) 393.

[13] MOUSSAÏD M., HELBING D., GARNIER S., JOHANSSON A., COMBE M. and THERAULAZ G., *Proc. R. Soc. London B*, **276** (2009) 2755.

[14] ZANLUNGO F., IKEDA T. and KANDA T., *EPL*, **93** (2011) 68005.

[15] ZHANG J., KLINGSCH W., SCHADSCHNEIDER A. and SEYFRIED A., *J. Stat. Mech. Theory E*, **2011** (2011) P06004.

[16] ZHANG J., KLINGSCH W., SCHADSCHNEIDER A. and SEYFRIED A., *J. Stat. Mech. Theory E*, **2012** (2012) P02002.

[17] HELBING D., *Complex Syst.*, **6** (1992) 391.

[18] BURSTEDDE C., KLAUCK K., SCHADSCHNEIDER A. and ZITTARTZ J., *Physica A*, **295** (2001) 507.

[19] BONABEAU E., *Proc. Natl. Acad. Sci. U.S.A.*, **99** (2002) 7280.

[20] HUGHES R. L., *Transp. Res. B-Methods*, **36** (2002) 507.

[21] SEYFRIED A., STEFFEN B. and LIPPERT T., *Physica A*, **368** (2006) 232.

[22] HELBING D. and MOLNÁR P., *Phys. Rev. E*, **51** (1995) 4282.

[23] Helbing D., Farkas I. and Vicsek T., *Nature*, **407** (2000) 487.

[24] Lakoba T. I., Kaup D. J. and Finkelstein N. M., *Simulation*, **81** (2005) 339.

[25] Oliveira C. L. N., Vieira A. P., Helbing D., Andrade J. S. jr. and Herrmann H. J., *Phys. Rev. X*, **6** (2016) 011003.

[26] Sticco I. M., Cornes F. E., Frank G. A. and Dorso C. O., *Phys. Rev. E*, **96** (2017) 052303.

[27] Kang Z., Zhang L. and Li K., *Appl. Math. Comput.*, **348** (2019) 355.

[28] Ikeda K. and Kim K., *J. Phys. Soc. Jpn.*, **86** (2017) 044004.

[29] Feliciani C., Murakami H. and Nishinari K., *PLoS ONE*, **13** (2018) e0208496.

[30] Vissers T., van Blaaderen A. and Imhof A., *Phys. Rev. Lett.*, **106** (2011) 228303.

[31] Vissers T., Wysocki A., Rex M., Löwen H., Royall C. P., Imhof A. and van Blaaderen A., *Soft Matter*, **7** (2011) 2352.

[32] Tarama S., Egelhaaf S. U. and Löwen H., *Phys. Rev. E*, **100** (2019) 022609.

[33] Kogler F. and Klapp S. H. L., *EPL*, **110** (2015) 10004.

[34] Sütterlin K., Wysocki A., Ivlev A. V., Räth C., Thomas H. M., Rubin-Zuzic M., Goedheer W. J., Fortov V. E., Lipaev A. M., Molotkov V. I.,

[35] Sarma U., Baruah S. and Ganesh R., *Phys. Plasmas*, **27** (2020) 012106.

Petrov O. F., Morfill G. E. and Löwen H., *Phys. Rev. Lett.*, **102** (2009) 085003.

[36] Shiwakoti N., Shi X. and Ye Z., *Safety Sci.*, **113** (2019) 54.

[37] Takimoto K., Tajima Y. and Nagatani T., *Physica A*, **308** (2002) 460.

[38] Helbing D., Farkas I. J. and Vicsek T., *Phys. Rev. Lett.*, **84** (2000) 1240.

[39] Nagatani T., *Physica A*, **388** (2009) 4973.

[40] Feliciani C. and Nishinari K., *Phys. Rev. E*, **94** (2016) 032304.

[41] See https://lammps.sandia.gov for the code.

[42] Glanz T. and Löwen H., *J. Phys.: Condens. Matter*, **24** (2012) 464114.

[43] Ikeda M., Wada H. and Hayakawa H., *EPL*, **99** (2012) 68005.

[44] Reichhardt C., Thibault J., Papanikolaou S. and Reichhardt C. J. O., *Phys. Rev. E*, **98** (2018) 022603.

[45] Marbach S. and Bocquet L., *J. Chem. Phys.*, **147** (2017) 154701.

[46] Marbach S. and Bocquet L., *Chem. Soc. Rev.*, **48** (2019) 3102.

[47] Zwanzig R., *Acc. Chem. Res.*, **23** (1990) 148.